Journal of Hydroscience and Hydraulic Engineering
Vol. 26, No.1 May, 2008, 11-27

DEPTH-AVERAGED NUMERICAL SOLVER OF MEANDERING RIVER FLOWS BY CIP-SOROBAN GRIDS IN CYLINDRICAL COORDINATE SYSTEM

By

Keisuke Yoshida

Interdisciplinary Graduate School of Science and Engineering, Tokyo Institute of Technology, Yokohama, Japan

and

Tadaharu Ishikawa

Interdisciplinary Graduate School of Science and Engineering, Tokyo Institute of Technology, Yokohama, Japan

SYNOPSIS

A new numerical solver is developed for a shallow-water flow model to simulate meandering river flows. This solver can investigate flows in curved river channels by means of the adaptive CIP-Soroban (CIP-S) scheme in a cylindrical coordinate system. Time development of depth-averaged water velocity and free-surface level is computed in the cylindrical (or orthogonal curvilinear) coordinate system without any transformation of the governing equations, and the advection term is calculated by the high-accuracy CIP scheme. The numerical accuracy of such a solver can be verified by the pure convection tests proposed by Zalesak and also examined by applying to a virtual meandering river flow. In comparison with the original CIP-S method in a Cartesian coordinate system as well as the boundary fitted coordinate (BFC) method, findings show that the proposed numerical solver performs well and that it can reasonably predict the main flow profile and water surface elevation.

INTRODUCTION

The clarification on the phenomena of unsteady free surface turbulent flows, sediment transport and morphological processes is one of the most important tasks in river engineering and related academic disciplines. The numerical prediction of these phenomena is very difficult for some reasons: the river flow is usually turbulent; the river bed and the bank line are irregular and can vary with time due to intermittent floods; and sediment transport phenomena are very complicated; this is because the whole phenomena are obviously of 3-dimensional nature. In recent years, the prevailing computational power has enabled us to conduct numerical predictions of these phenomena in less time and more cheaply than ever before. This background has motivated the 3-D computations of the complex phenomena, carried out by several hydraulic researchers, e.g., see Wu *et al.* (8) and Olsen (7).

Although the several 3-D simulation models have been developed so far, hydraulic engineers and management designers engaged in the practical river engineering problems are still demanding reasonable and accurate 2-D simulation models for some preliminary analyses and parametric trade-off studies. Such kinds of deliberations are usually required in the planning of river engineering projects and decision making on the feasibility evaluation. The

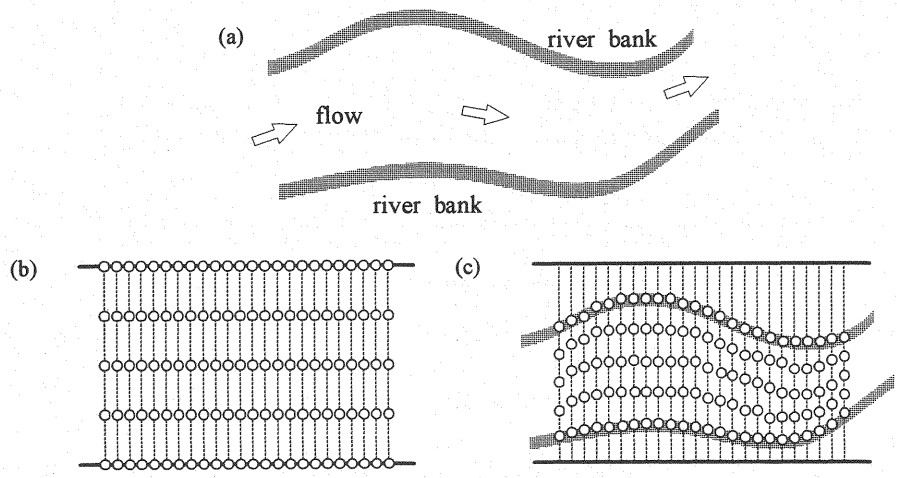

Figs.1 Schematic illustration of irregular riverbank topography and adptive numerical grids
(a) riverbank topology, (b) abacus (Soroban grid) and (c) adaptive Soroban grid
○ : numerical grid (Soroban grid), ... : Soroban line

reason for employing the 2-D models is that they require the sufficient discussion of the pros and cons in a relatively short time. This necessitates investigating the effects of the projects by means of the hydraulic simulations. Furthermore, it is not computationally efficient to use the 3-D model in dealing with the overall river from the upstream alluvial region to the downstream river mouth. Therefore, among the 2-D models, the realistic researchers in their early works (see e.g., Engelund (1) and Kalkwijk & De Vriend (4)) developed the shallow water model that is suitable for the simulation of river flows and is also based on the depth-integrated Reynolds-averaged equations. In addition, for some decades, several outstanding practical models that can account for the mean flows and morphology in natural meandering rivers have been developed. For instance, Ikeda & Nishimura (2) and Johannesson & Parker (3) pointed out the significance of the so-called secondary currents in the river bends, and they consider the influence of the momentum transfer due to the currents in their 2-D models. Ye & MaCorquodale (11) incorporated the river bank- (or boundary-) fitted coordinate system in their numerical models. Furthermore, Nagata *et al.* (5) have developed the 2-D numerical model which can treat the movable banks due to erosion and deposition processes.

Recent models frequently adopt the numerical technique with the river bank or boundary fitted coordinate (BFC) system in the practical simulations: hereafter, we refer to it as the BFC method. In the numerical simulation, this coordinate system has both advantages and drawbacks. For example, it is generally known that it can avoid the poor resolution of the grids near the irregular river banks, such as a stair-stepped approximation, so that it can save the numerical cost by which we are accustomed to refine the grids near the banks. However, this method requires the geometrical transformation of the governing equations, and the resulting equations represent a complicated mathematical form. Moreover, it has been generally noted that the BFC method improves the numerical cost and accuracy in the computation of the flows within the complex boundaries. However, it was pointed out by Yabe *et al.*(10) that in this BFC method, the numerical transformation of governing equations from the orthogonal to the non-orthogonal coordinate system results in the severe reduction of numerical accuracy, especially caused by numerical diffusion generated in the convection terms of the equations. Therefore, Yabe *et al.*(10) proposed a new type of boundary-fitted grid system known as the 'Soroban grid', in which the accurate convection scheme by the CIP method (see Yabe *et al.*(9)) is easily applied: hereafter, this technique is referred to as the CIP-Soroban (CIP-S) method. Figures 1 show the schematic illustration of the bank topography and this grid system. This system

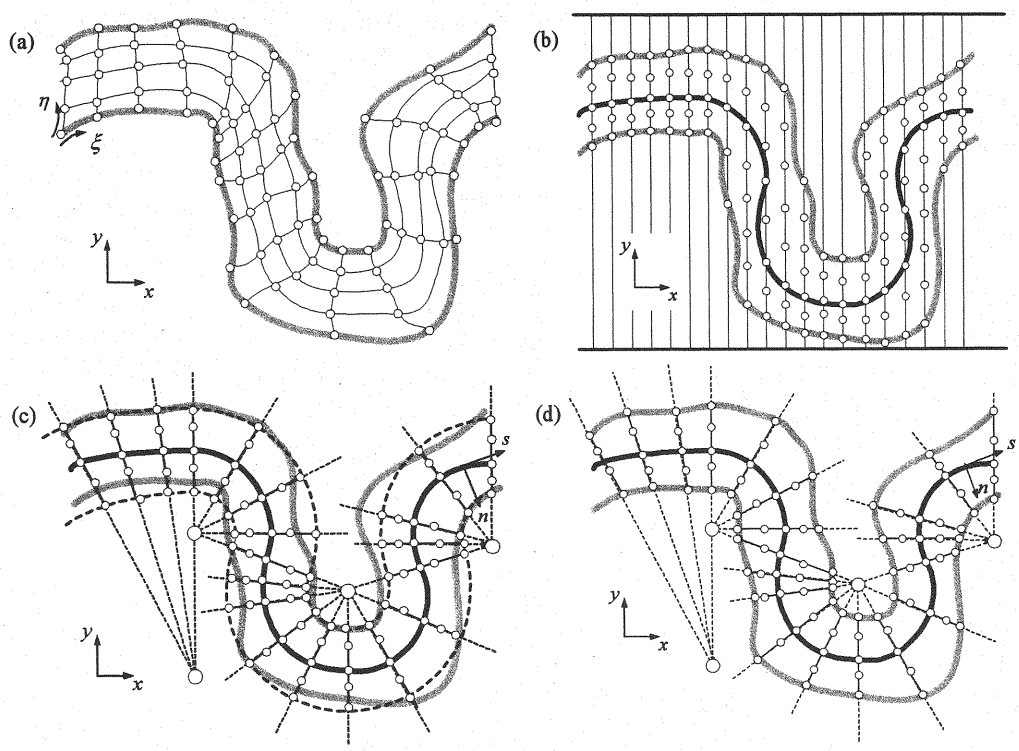

Figs.2 Bend topography and bankline- (boundary-) fitted & approximated numerical grids
(a) BFC grids, (b) original Soroban grids, (c) successive cylindrical grids and (d) proposed grids
(; bankline, ; cylindrical grid line, ; channel center line, ; radial line
;cross-section of channel, ○ ; center of circle of curvature of bend, o ; grid points)
(x, y ; Cartesian, s, n ;orthogonal curvilinear and ξ, η ; boundary fitted coordinate system)

consists of the several straight vertical lines (drawn as the dotted lines in Figs.1) and some grid points (drawn as the open circle) located along these lines like an abacus – Soroban in Japanese. This straight line is hereafter referred to as the Soroban line. The span of the each line and the number of the points in each line can be irregular in the idea of the original paper, and the location of each grid point is set up so that the grids at the both ends of each line are put on the both bank lines. Thus, the numerical grid shown here represents a semi-structured feature; the Soroban line (abacus line) is regularly aligned parallel to each other, and the Soroban grids can be arbitrarily arranged in order to adjust the location of the grids in the boundaries. As shown in Figs.1 (c), the resulting adaptive grid system can be developed for the river bend topography.

FUNDAMENTAL IDEA OF NEW FLOW MODEL & OBJECTIVE OF THIS STUDY

Figures 2 show the example of the river bend topography with large curvature and the comparison of representation of numerical grids fitted to the irregular bank line with four systems; (a) the conventional BFC system, (b) the original Soroban grid system, (c) the successively connected cylindrical coordinate system or the orthogonal curvilinear coordinate (OCC) system and (d) the proposed grid system. Figs.2 (b) shows that the river bends with large curvature are no longer described in the ordinary way as in the example in Figs.1(c) by means of the original Soroban grid system, because it is not convenient for the numerical modeler that the curved channel way (or the

channel center line) is partly parallel to the Soroban line and that the bank line is partly represented by the multi-value function of the x axis. As a result, it means that the simple representation of the channel bend topography with large curvature is realized by (a) the BFC system and by (c) the OCC system. As for the OCC system, the physical boundary or bank line is approximately composed by the several pieces of the circular arcs with different curvature, while the complicated bank line is not always exactly in correspondence to the circular arc, since each numerical grid is located in the certain arc at the boundaries. Thus, evidence clearly shows that the complicated boundary (bank-line) observed in the natural river is not always represented only by the conventional numerical grids in the OCC system, but by the other combined numerical grids. On the other hand, the grid system proposed in this study (Fig.2 (d)) is represented by combining the Soroban grids with the OCC; it should be noted in the new system that the Soroban line is no longer just parallel to each other in the Cartesian coordinate system, but in the OCC system. Consequently, the numerical grids at both ends in each Soroban line can be always located on the bank line.

The advantage of using the proposed new system is as follows. Since the new system is composed by the orthogonal base, it can allow us to directly utilize the accurate convection schemes such as the CIP method, which has been conventionally used by many researchers in the Cartesian coordinate system. In addition, we can adopt this coordinate system to the irregular physical boundary. The reason for this is that this system employs both regularity in the structured grids and flexibility to the irregular boundaries in the unstructured grids.

The purpose of this study is to propose the new numerical solver for the meandering river flows with the adaptive Soroban grids in the cylindrical coordinate system, to verify the accuracy of the CIP scheme in the cylindrical coordinate system in the pure advection problem suggested by the Zalesak (12), and to investigate the performance of the model in the shallow water flows, compared both with the original CIP-S method and with the BFC method. This study focuses on the fundamental investigation of applicability of the new solver in shallow water flows. Therefore, the momentum transfer due to the secondary currents which is critical in the practical flows is not considered, however it will be examined in further investigations.

NUMERICAL PROCEDURE

Governing equations

The following assumptions are made in the model developed here: 1) incompressible Newtonian fluid; 2) constant viscosity; 3) hydrostatic pressure distribution along the water depth; 4) negligible wind shear on the water surface. With these assumptions, the 2-D governing equations of the open-channel flows are obtained by integrating the Reynolds-averaged continuity and Navier-Stokes equations from the channel bottom to the water surface. These equations are described as conservative forms in a generalized (or boundary fitted) curvilinear coordinate system as follows (see e.g., Nagata *et al.* (5)):

Continuity Equation

$$\frac{\partial}{\partial t}\left(\frac{h}{J}\right)+\frac{\partial}{\partial \xi}\left(\frac{h\hat{U}}{J}\right)+\frac{\partial}{\partial \eta}\left(\frac{h\hat{V}}{J}\right)=0 \tag{1}$$

Momentum Equations

$$\begin{aligned}&\frac{\partial}{\partial t}\left(\frac{Q^{\xi}}{J}\right)+\frac{\partial}{\partial \xi}\left(\frac{Q^{\xi}\hat{U}}{J}\right)+\frac{\partial}{\partial \eta}\left(\frac{Q^{\xi}\hat{V}}{J}\right)-\frac{M}{J}\left(\hat{U}\frac{\partial \xi_x}{\partial \xi}+\hat{V}\frac{\partial \xi_x}{\partial \eta}\right)-\frac{N}{J}\left(\hat{U}\frac{\partial \xi_y}{\partial \xi}+\hat{V}\frac{\partial \xi_y}{\partial \eta}\right)\\&=-gh\left(\frac{\xi_x^2+\xi_y^2}{J}\frac{\partial H}{\partial \xi}+\frac{\xi_x\eta_x+\xi_y\eta_y}{J}\frac{\partial H}{\partial \eta}\right)-\frac{\tau_b^{\xi}}{\rho J}+\mathrm{Rey}_{\xi}\end{aligned} \tag{2a}$$

$$\frac{\partial}{\partial t}\left(\frac{\overline{Q^\eta}}{J}\right)+\frac{\partial}{\partial \xi}\left(\frac{\overline{Q^\eta \hat{U}}}{J}\right)+\frac{\partial}{\partial \eta}\left(\frac{\overline{Q^\eta \hat{V}}}{J}\right)-\frac{M}{J}\left(\hat{U}\frac{\partial \eta_x}{\partial \xi}+\hat{V}\frac{\partial \eta_x}{\partial \eta}\right)-\frac{N}{J}\left(\hat{U}\frac{\partial \eta_y}{\partial \xi}+\hat{V}\frac{\partial \eta_y}{\partial \eta}\right)$$
$$=-gh\left(\frac{\xi_x\eta_x+\xi_y\eta_y}{J}\frac{\partial H}{\partial \xi}+\frac{\eta_x^2+\eta_y^2}{J}\frac{\partial H}{\partial \eta}\right)-\frac{\tau_b^\eta}{\rho J}+\mathrm{Rey}_\eta \tag{2b}$$

$$\mathrm{Rey}_\xi=\left(\frac{\xi_x^2}{J}\frac{\partial}{\partial \xi}+\frac{\xi_x\eta_x}{J}\frac{\partial}{\partial \eta}\right)(-\widetilde{\overline{U'U'}}h)$$
$$+\left(\frac{2\xi_x\xi_y}{J}\frac{\partial}{\partial \xi}+\frac{\xi_x\eta_y+\xi_y\eta_x}{J}\frac{\partial}{\partial \eta}\right)(-\widetilde{\overline{U'V'}}h)+\left(\frac{\xi_y^2}{J}\frac{\partial}{\partial \xi}+\frac{\xi_y\eta_y}{J}\frac{\partial}{\partial \eta}\right)(-\widetilde{\overline{V'V'}}h) \tag{3a}$$

$$\mathrm{Rey}_\eta=\left(\frac{\xi_x\eta_x}{J}\frac{\partial}{\partial \xi}+\frac{\eta_x^2}{J}\frac{\partial}{\partial \eta}\right)(-\widetilde{\overline{U'U'}}h)$$
$$+\left(\frac{\xi_x\eta_y+\xi_y\eta_x}{J}\frac{\partial}{\partial \xi}+\frac{2\eta_x\eta_y}{J}\frac{\partial}{\partial \eta}\right)(-\widetilde{\overline{U'V'}}h)+\left(\frac{\xi_y\eta_y}{J}\frac{\partial}{\partial \xi}+\frac{\eta_y^2}{J}\frac{\partial}{\partial \eta}\right)(-\widetilde{\overline{V'V'}}h) \tag{3b}$$

where t = time; ξ and η = boundary fitted coordinates; x and y = Cartesian coordinates; h = local water depth; M and N = $x-$ and $y-$ components of discharge flux; ρ = fluid density; g = gravity acceleration; H = water level; $-\widetilde{\overline{U'U'}}$, $-\widetilde{\overline{U'V'}}$ and $-\widetilde{\overline{V'V'}}$ = Cartesian components of depth-averaged Reynolds stress tensors; ξ_x, η_x, ξ_y and η_y = metrics; J = Jacobian which is defined as $J=1/\left(x_\xi y_\eta - x_\eta y_\xi\right)$; $\hat{U}$ and $\hat{V}$ = contravariant components of velocity vectors; Q^ξ and Q^η = contravariant components of discharge fluxes; and τ_b^ξ and τ_b^η = contravariant components of bottom shear stress vectors. The superscript ' denotes the time fluctuation component of velocity; the over bar $\bar{}$ = time-averaging operator; and the superscript tilde $\tilde{}$ = depth-averaging operator. By means of the chain rule, the contravariant components are defined as follows:

$$\hat{U}=\xi_x U+\xi_y V;\quad \hat{V}=\eta_x U+\eta_y V \tag{4a}$$

$$Q^\xi=\xi_x M+\xi_y N;\quad Q^\eta=\eta_x M+\eta_y N;\quad \tau_b^\xi=\xi_x\tau_{bx}+\xi_y\tau_{by};\quad \tau_b^\eta=\eta_x\tau_{bx}+\eta_y\tau_{by} \tag{4b}$$

where U and V = $x-$ and $y-$ components of velocity vectors; and τ_{bx} and τ_{by} = $x-$ and $y-$ components of bottom shear stress vectors.

The governing equations mentioned above are transformed by a fundamental covariant tensor which denotes the geometrical relationship between the orthogonal curvilinear system and the generalized coordinate one, and then these pre-described equations are replaced by the simple form of the following equations:

$$\frac{\partial h}{\partial t}+\frac{1}{1+\sigma n}\frac{\partial hu}{\partial s}+\frac{1}{1+\sigma n}\frac{\partial}{\partial n}\left\{\left(1+\sigma n\right)hv\right\}=0 \tag{5}$$

$$\frac{\partial u}{\partial t}+\frac{u}{1+\sigma n}\frac{\partial u}{\partial s}+v\frac{\partial u}{\partial n}+\frac{\sigma uv}{1+\sigma n}=-\frac{g}{1+\sigma n}\frac{\partial H}{\partial s}-\frac{\tau_{bs}}{\rho h}+\frac{\mathrm{REY}_s}{h} \tag{6a}$$

$$\frac{\partial v}{\partial t}+\frac{u}{1+\sigma n}\frac{\partial v}{\partial s}+v\frac{\partial v}{\partial n}-\frac{\sigma u^2}{1+\sigma n}=-g\frac{\partial H}{\partial n}-\frac{\tau_{bn}}{\rho h}+\frac{\mathrm{REY}_n}{h} \tag{6b}$$

$$\mathrm{REY}_s=\frac{1}{1+\sigma n}\frac{\partial}{\partial s}\left(-\widetilde{\widetilde{u'u'}}h\right)+\frac{\partial}{\partial n}\left(-\widetilde{\widetilde{u'v'}}h\right)+\frac{2\sigma}{1+\sigma n}\left(-\widetilde{\widetilde{u'v'}}h\right) \tag{7a}$$

$$\mathrm{REY}_n=\frac{1}{1+\sigma n}\frac{\partial}{\partial s}\left(-\widetilde{\widetilde{u'v'}}h\right)+\frac{\partial}{\partial n}\left(-\widetilde{\widetilde{v'v'}}h\right)-\frac{\sigma}{1+\sigma n}\left(-\widetilde{\widetilde{u'u'}}h\right)+\frac{\sigma}{1+\sigma n}\left(-\widetilde{\widetilde{v'v'}}h\right) \tag{7b}$$

where s and n = orthogonal curvilinear coordinates; u and v = $s-$ and $n-$ components of velocity vectors; σ = local curvature along the channel coordinate (s axis); τ_{bs} and τ_{bn} = bottom shear stress vectors; and $-\widetilde{\widetilde{u'u'}}$, $-\widetilde{\widetilde{u'v'}}$ and $-\widetilde{\widetilde{v'v'}}$ = orthogonal curvilinear components of depth-averaged Reynolds stress tensors . The Eqs.6 are not described in the conservative form, so that the advantage of the aforementioned CIP method can be directly utilized in this orthogonal coordinate system.

Closure model of quantifying stress terms

To solve the Eqs.1 ~ Eqs.4 by the BFC method and the Eqs.5 ~ Eqs.7 by the CIP-S method as a closed system, the stress terms on the right-hand side of the equations have to be expressed as the explicit forms of the depth-averaged velocity and the water depth. The bottom shear stresses $\tau_{bx}, \tau_{by}, \tau_{bs}$ and τ_{bn} are modeled by the Manning formula on uniform flows. Moreover, the laminar viscous stresses and turbulent stresses can be quantified based on the Boussinesq eddy-viscosity concept. The depth-averaged Reynolds stress tensors, $-\widetilde{\widetilde{U'_iU'_j}}$ and $-\widetilde{\widetilde{u'_iu'_j}}$, are evaluated by the following simple method in each coordinate system:

$$-\widetilde{\widetilde{U'U'}}=2D_h\frac{\partial\tilde{U}}{\partial x}-\frac{2}{3}k;\quad -\widetilde{\widetilde{U'V'}}=D_h\left(\frac{\partial\tilde{U}}{\partial y}+\frac{\partial\tilde{V}}{\partial x}\right);\quad -\widetilde{\widetilde{V'V'}}=2D_h\frac{\partial\tilde{V}}{\partial y}-\frac{2}{3}k \tag{8a}$$

$$-\widetilde{\widetilde{u'u'}}=D_h\left(\frac{\partial\tilde{u}}{\partial n}+\frac{\sigma\tilde{v}}{1+\sigma n}\right)-\frac{2}{3}k;\quad -\widetilde{\widetilde{u'v'}}=D_h\left(\frac{\partial\tilde{u}}{\partial n}+\frac{\partial\tilde{v}}{\partial s}-\frac{\sigma\tilde{u}}{1+\sigma n}\right);\quad -\widetilde{\widetilde{v'v'}}=2D_h\frac{\partial\tilde{v}}{\partial n}-\frac{2}{3}k \tag{8b}$$

where D_h = horizontal kinematic eddy viscosity; and k = depth-averaged turbulent kinetic energy derived from integration of the empirical formula proposed by Nezu & Nakagawa (6):

$$k=2.07U_*^2 \tag{9}$$

where U_* = local friction velocity.

Numerical solution by BFC method

(1) Numerical schemes

The Eqs.1 ~ Eqs.3 are discretized by means of the finite difference method using the conservative concept employed in the finite volume method. Time development of depth-averaged velocity and water depth is computed

by the explicit Adams-Bashforth scheme with second-order accuracy. The spatial derivatives are discretized by the second-order central scheme, with the exception of the advection terms which are discretized by the first-order upwind scheme.

In the typical BFC method, the independent variables are usually mapped from the physical space to the computational one. In every computation cell, the grid size is set at 1.0 in each direction. To avoid the well-known numerical oscillation on non-staggered grids, the variables of flux are located at the cell boundary.

(2) Boundary condition

The boundary conditions needed for solving the Eqs.1 ~ Eqs.3 are the discharge hydrograph across the channel at the upstream end and water surface elevation at the downstream end in the case of the subcritical flows. In addition, the slip condition for the depth-averaged velocity parallel to the boundary wall is adopted at both sides of the channel, so that the velocity perpendicular to the wall is zero.

Numerical solution by CIP-Soroban method

(1) Numerical schemes

The non-conservative form of Eqs.5 ~ Eqs.7 can be discretized by the finite difference method in which we can employ the advantage of the CIP scheme. Time development of the depth-averaged velocity and the water depth is computed by the time-splitting CIP scheme with third-order accuracy in time and space. By progressing the calculation in almost the same manner as the original algorithm of the CIP scheme, the governing Eqs.5 ~ Eqs.7 can be split into the two phases, that is to say, advection and non-advection phases. In this study, the time-splitting operation is applied only to the Eqs.6:

(Advection phase)

$$\frac{\partial u}{\partial t}+\frac{u}{1+\sigma n}\frac{\partial u}{\partial s}+v\frac{\partial u}{\partial n}=0\,;\qquad \frac{\partial v}{\partial t}+\frac{u}{1+\sigma n}\frac{\partial v}{\partial s}+v\frac{\partial v}{\partial n}=0 \tag{10}$$

(Non-advection phase)

$$\frac{\partial h}{\partial t}+\frac{1}{1+\sigma n}\frac{\partial hu}{\partial s}+\frac{1}{1+\sigma n}\frac{\partial}{\partial n}\left\{(1+\sigma n)hv\right\}=0 \tag{11}$$

$$\frac{\partial u}{\partial t}=-\frac{\sigma uv}{1+\sigma n}-\frac{g}{1+\sigma n}\frac{\partial H}{\partial s}-\frac{\tau_{bs}}{\rho h}+\frac{\mathrm{REY}_s}{h}\,;\quad \frac{\partial v}{\partial t}=\frac{\sigma u^2}{1+\sigma n}-g\frac{\partial H}{\partial n}-\frac{\tau_{bn}}{\rho h}+\frac{\mathrm{REY}_n}{h} \tag{12}$$

The Eqs.10 are composed of the 2-D parabolic type of expressions from the mathematical viewpoint, so that these equations can be numerically solved by the accurate CIP scheme. On the contrary, the Eqs.12 are discretized by the central differencing scheme, since the numerical diffusion appears typically and degenerates the numerical accuracy, especially in the advection terms.

To progress the time development of the flow fields, the present model makes use of the almost same method as the original approach supposed by Yabe *et al.* (9). The main feature of this method is solving the above equations in three steps to keep the numerical stability, on the basis of the fractional step implicit algorithm. The process is carried out as follows: The first step is involves computing the advection-phase velocity u^*, v^* in the Eqs.10 from the value of u^n, v^n, h^n by the CIP scheme. Here, the superscript n refers to the time level $n\times\Delta t$ (Δt = time increment). The second step is to compute the provisional velocity u^{**}, v^{**} with use of u^*, v^* in the Eqs.12 without considering the gradient terms of the water level $\partial H/\partial s$ and $\partial H/\partial n$. The third step (or propagation step) involves

computing the Eqs.11 and Eqs.12 iteratively with the given value of u^{**}, v^{**} and h^n, until the convergence error is minimized within the prescribed threshold value ε, and also to obtain the renewal velocity field u^{n+1}, v^{n+1} and water depth h^{n+1} in the next step. Since the Eqs.11 and Eqs.12 include the nonlinear terms, the successive over-relaxation (SOR) method with a relaxation factor less than 1.0 is adopted in this solution.

In the case of irregular grid location observed in the Soroban grid system as shown in Fig.1(c), the original methodology of the CIP scheme (called as Type-A) becomes unavailable. In such a case, the Type-M scheme (see Yabe *et al.*(10)), which is one of the varieties of the CIP schemes, is convenient. Actually, this type of scheme is composed of the original 1-D CIP scheme along the Soroban line and the linear interpolation spanned across the Soroban line. Since the linear interpolation is conducted along the direction normal to the advection, the degradation of accuracy does not occur so much. In this study, the Type-M scheme is incorporated in the computation.

(2) Boundary condition

The boundary condition in the CIP-S method is the same as that in the BFC method, except for the side-wall boundary. In the paper dealing with the original CIP-S method, the boundary condition is not explicitly suggested and it actually depends on the case-by-case issue. In this study, the boundary condition is applied to the model by the following rule:

$$\frac{\partial n_k}{\partial t} + \frac{u}{1+\sigma n}\frac{\partial n_k}{\partial s} = v \tag{13}$$

where n_k ($k = right\ or\ left$) represents the value of the n axis at the side-walls. The Eq.13 means that the water body with the finite water depth moves near the waterfront, following the kinematic boundary condition at the side-walls. The upper rule is also widely known when dealing with the free-surface condition; namely, the numerical grid at the side-wall boundary ($n = n_k$) is moved along the Soroban line driven by the velocity (u,v) near the side-wall, and the physical value on the grid is renewed and replaced by the value estimated at the upwind point of the grid. Here, the location of the upwind point is calculated by the CIP scheme.

APPLICATIONS & DISCUSSIONS

Verification of CIP scheme in cylindrical coordinate system

The 2-D scalar convection technique of the CIP scheme in the cylindrical coordinate is investigated in this section. The original CIP scheme was developed in the orthogonal coordinate system, and the calculation of the convection terms is performed based on the semi-Lagrangian concept used in the same solution as the Leith scheme. Figure 3 illustrates the concept in the Cartesian coordinate system and the OCC system. The four points named as A, B, C and D represent the numerical grids and the physical value is computed at each point in each time step. The open circle at the point A is the corresponding location where the scalar value is to be obtained at next computation time step. From a theoretical viewpoint, it is obvious that the filled circle represents the origin from which the profile of the scalar value is convected to the point A by the local velocity. In the CIP scheme, the profile at the point E is interpolated by the cubic function using the information of the scalar value f and its spatial derivatives f_x and f_y. Therefore, the CIP scheme has the third-order accuracy in time and space.

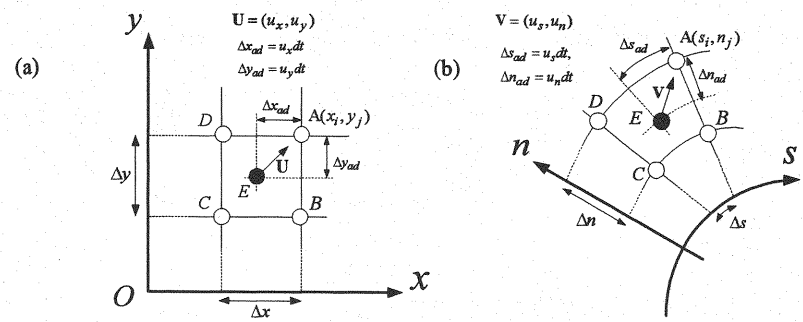

Figs.3 Illustration of semi-Lagrange concept in CIP scheme (a) in the Cartesian coordinate (x, y) and (b) in the cylindrical coordinate (s, n)

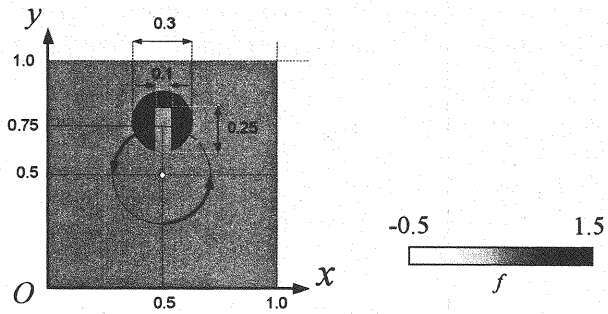

Figs.4 Initial profile of the scalar value f in pure convection problem (PCP)

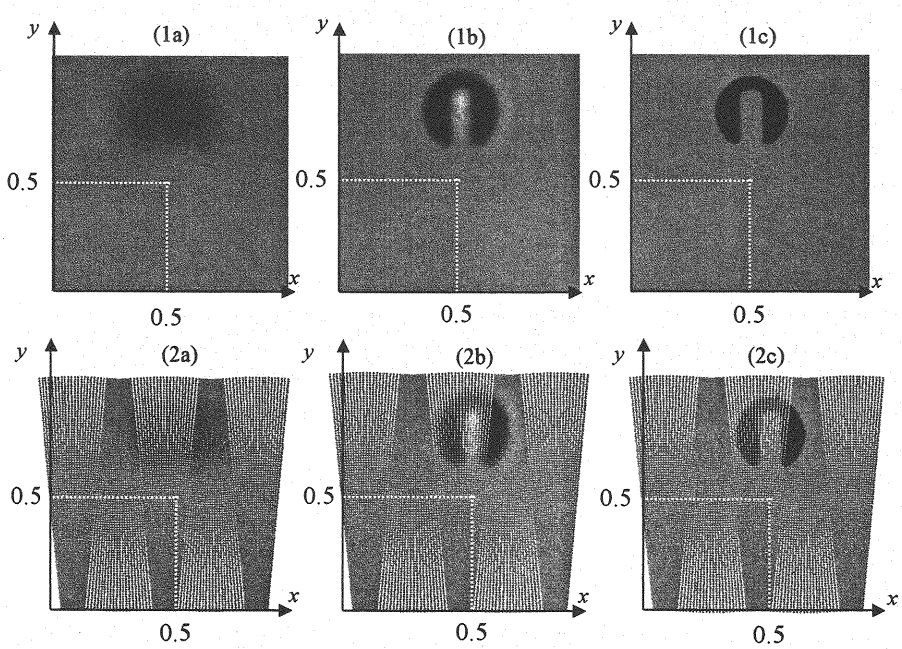

Figs.5 Numerical results after a 1-round trip in PCP
(1a) 1st order upwind, Cartesian, (1b) 3rd order upwind, Cartesian, (1c) CIP, Cartesian,
(2a) 1st order upwind, Cylindrical, (2b) 3rd order upwind, Cylindrical and (2c) CIP, Cylindrical

Table 1 Numerical results of conservation factor F and deviation factor ε in PCP

	Cartesian Coordinate System			Orthogonal Curvilinear Coordinate System		
	1st upwind	3rd upwind	CIP	1st upwind	3rd upwind	CIP
F	1.00	1.02	1.01	1.0	1.02	1.02
λ	0.038	0.017	0.010	0.038	0.017	0.009

Figure 4 shows the initial profile of the well-known pure convection problem (PCP) proposed by Zalesak (12) in which the scalar value f is transferred by the solid body revolution. At the initial states, the inside value of the cut-out cylinder is set at 1.0 and the outside is 0.0. The grid numbers are 102×102 along the 2-D axes. The rotation speed is determined so that the Courant number is about 0.1. Figures 5 (1a) ~ (1c) & (2a) ~ (2c) show the results after one-round trip by a) the first-order upwind scheme, b) the 3rd-order upwind scheme and c) the CIP scheme, in the Cartesian coordinate system as well as in the OCC system. The computation domain in the OCC system is formed to be approximately the square region with five series of cylindrical coordinate system. The theoretical result of this problem should be the initial profile f_{ini} because of one-round revolution. Figure 6 shows a comparison of numerical results of the vertical scalar profile of f at the specific cross-section (x = 0.5) after a one-round trip in PCP, and we introduce the conservation factor F and the deviation factor λ are evaluated by the following formulae and each value is descried in the Table1:

$$F = \left(\sum_{i,j} f_{cal}(i,j) - \sum_{i,j} f_{theory}(i,j) \right) \Big/ \sum_{i,j} f_{theory}(i,j) \tag{14}$$

$$\lambda = \sqrt{\left(\sum_{i,j} \left[f_{cal}(i,j) - f_{theory}(i,j) \right]^2 \right)} \Big/ \sum_{i,j} f_{theory}(i,j) \tag{15}$$

where $f_{cal}(i,j)$ denotes the two-dimensional scalar profile calculated by each numerical scheme, $f_{theory}(i,j) = f_{ini}(i,j)$ means the theoretical or initial scalar profile, and (i,j) shows the index defined in the 2-D computation domain. The integration is numerically conducted all over the 2-D computation domain. It should be noted that the results by the first-order upwind scheme show the numerical diffusion in both coordinate systems, and that the results by the third-order upwind scheme show the numerical oscillation in both coordinate systems, however, findings reveal that the results by the CIP scheme are consistent with the theoretical solution and show that the CIP scheme is the better solver for the purpose of calculating the convection terms.

Comparison of CIP-Soroban method with BFC method

(1) Virtual meandering open channel

This section investigates the performance of the proposed solver of the shallow water flows. Figure 7 shows the schematic illustration of a virtual meandering open channel and the arrangement of numerical grids used in the CIP-S method. There are two types of numerical grids shown in the figure. In the case of the orthogonal curvilinear coordinate, the Soroban line is normal to the longitudinal direction. This channel consists of the about 13m-long bend way and 2.0m-long upstream straight way. The channel width B is $\sqrt{2}$ m and the radius of curvature along the

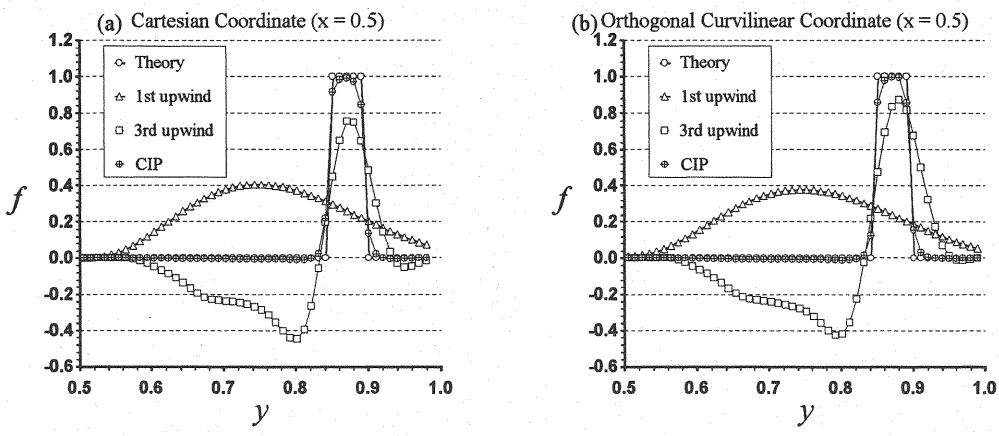

Figs.6 Comparison of numerical results of vertical profile of f at x = 0.5 after a 1-round trip in PCP (a; Cartesian coordinate system vs. b; Orthogonal curvilinear coordinate system)

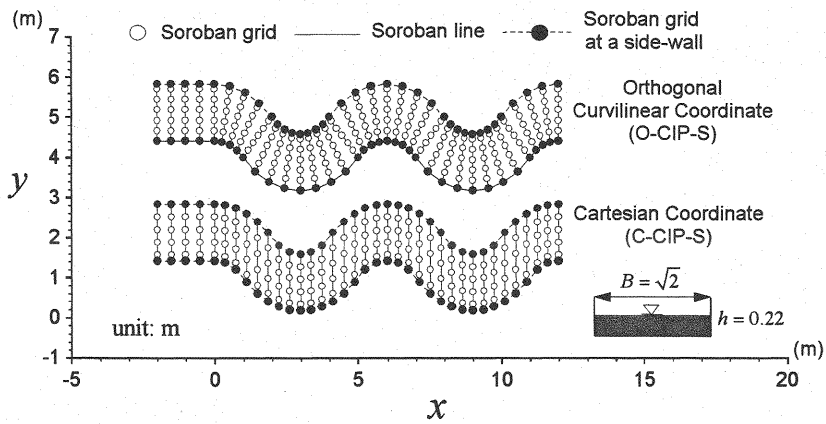

Fig.7 Schematic sketch of virtual meandering open channel and arrangement of numerical grids

channel axis s in the bend is $3/\sqrt{2}$ m.

(2) Numerical condition

The grid number is 82×10, with 82 sections in the streamwise direction or x-direction and 10 grids in the cross-sectional direction or y-direction. The discharge of the channel inlet Q_{in} is 0.1 m^3/s and the outlet water depth H_{out} is set at 0.22m. The channel slope is set zero in each section. The initial condition is the static water. The shear stress on the bed is evaluated by the Manning formula and the coefficient is set at 0.032. In addition, the horizontal kinetic viscosity D_h is determined by the Richardson's empirical formula.

The channel has a flat bottom and vertical side-walls, which means the water front line is fixed at the wall. However, only in the computation by the CIP-S method, the water front line is kept flexible according to the Eq.13 and movable due to the flow discharge and water depth. Therefore, the vertical side-wall with a right angle is treated numerically as a steep slope defined by the exponential function. If the grids at the side-walls are renewed by the hydrograph and the water level at the downstream end, then the grid locations are rearranged so that the grid space is

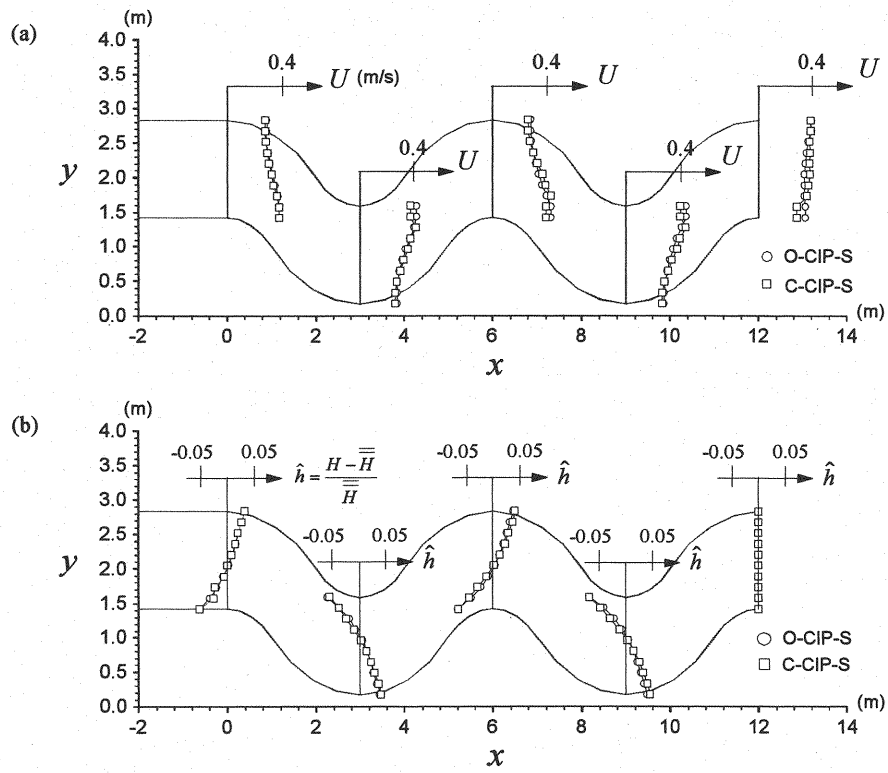

Figs.8 Numerical results of (a) the depth-averaged velocity U in the x direction and (b) the normalized water elevation $\hat{h}$ at five cross-sections along the channel ($\overline{\overline{H}}$: cross-sectionally averaged water depth)

kept regular and similar to each other in each Soroban line.

(3) Numerical results

Figures 8 show the numerical results of a) the depth-averaged velocity in the x direction and b) the deviation of water level from the cross-sectionally averaged water depth $\overline{\overline{H}}$ at five sections along the channel. The data are obtained by the original CIP-S method in the Cartesian coordinate system (C-CIP-S) and by the proposed method (O-CIP-S). It was found that the data are consistent to each other, and that both numerical results are reasonable, since the velocity near the inside wall is predominant, compared with the one near the outside wall and that the water elevation decreases near the inside wall. Figures 9 show a detailed comparison of the numerical results of the depth-averaged velocity in the x direction. The caption (N_x, N_y) in the figure denotes the 2-D grid number used in each method. The figure shows the results by the BFC method with more grids becomes close to that by the O-CIP-S method and the C-CIP-S method. In general, the numerical calculations using much more grids show better performance in the finite difference (volume) method, no matter what numerical method we adopt. It is natural that we can consider this concept is also true in the Fig.9. Thus, this is why the numerical results in the Fig.9 explain the priority of the O-CIP-S method and the C-CIP-S method to the BFC method in terms of the numerical accuracy. Moreover, the results by the C-CIP-S method are different from those by the O-CIP-S method near the wall. The reason for this is the discretizaiton of the equations near the curved wall by the finite difference method is difficult in

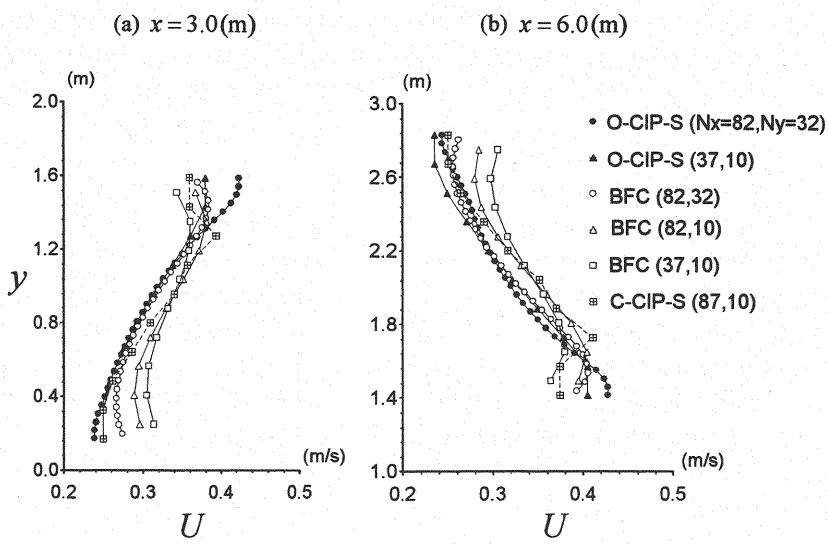

Figs.9 Detailed numerical results of Figs.8 (a) at x=3.0(m) and 6.0(m)

(N_x, N_y) : 2-D numerical grid number

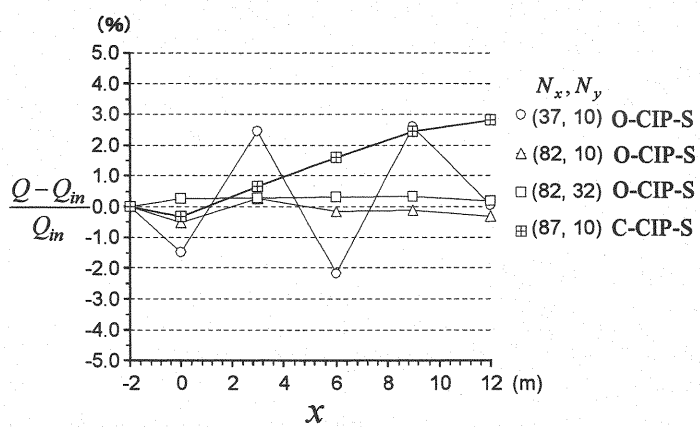

Fig.10 Comparison of deviation of the flow discharge Q at each section between the methods with various grids

Q_{in} : water discharge at the upstream end

the C-CIP-S method. This problem is caused by the directional discordance between the normal vector to the side wall and the Soroban line, and we will be able to overcome this kind of difficulty by using the local boundary fitted coordinate in the calculation of the coupling operation between the continuity equation and the momentum equations. This issue will be flexibly closed and discussed in detail in our next study.

Figure 10 shows the normalized deviation of the discharge Q at each section from the inlet discharge Q_{in}. The discharge is calculated by the trapezoid formula. The data of the BFC method is omitted in the figure because in the BFC method the discharge is almost completely conserved within the given threshold value. This is because the governing equations are discretized by the finite volume method. On the other hand, the CIP-S method uses the finite difference method so that the conservation is not always guaranteed. It should be pointed out in the Fig.10 that

the conservation is almost completely satisfied in the O-CIP-S method by using more numerical grids; however, the deviation was found to be increasing in using the C-CIP-S method. This is because a problem occurs in the discretizaiton of the governing equations near the curved side-walls in the C-CIP-S method.

CONCLUSION

The new numerical solver is developed for the shallow-water model to simulate meandering river flows. This solver can investigate the flows in the curved rivers by means of the adaptive CIP-Soroban (CIP-S) scheme in the cylindrical coordinate system. A bench mark test of the performance of the scheme both in the pure convection problem and in the shallow water flows was carried out. Findings revealed that the proposed model yields reasonable results in each test compared with the conventional schemes and models. The current solver proposed in this study has some aspects that need to be improved for the practical purposes in detail, such as conservation of water body and flexibility to the arbitrary bank shapes. Upgrading the model is necessary with e.g., the effects of secondary currents. Such revisions will be examined in further studies.

ACKNOWLEDGEMENTS

This research was partially supported by the Ministry of Education, Science, Sports and Culture, Grant-in-Aid for Young Scientists (B). The authors would like to thank the government authority for funding this work.

REFERENCES

1. Engelund, F. : Flow and bed topography in channel bends, *Proc. ASCE, J. Hydr. Div.*, Vol.100, HY11, pp. 1631-1647, 1974.
2. Ikeda, S. and Nishimura, T.: Flow and bed profile in meadering sand-silt rivers, *J. Hydr. Eng., ASCE*, Vol.112, No.7, pp.562-579, 1986.
3. Johannesson, H. and Parker, G. : Secondary flow in mildly sinuous channel, *J. Hydr. Eng., ASCE*, Vol.115, No.3, pp.289-308, 1989.
4. Kalkwijk, J. P. T., and De Vriend, H. J. : Computation of the flow in shallow river bends, *J. Hydr. Res.*, Vol.18, No.4, pp.327-342, 1980.
5. Nagata, N., Hosoda, T. and Muramoto, Y.: Numerical analysis of river channel processes with bank erosion, *J. Hydr. Eng.*, Vol.126, No.4, pp.243-252, 2000.
6. Nezu, I. and Nakagawa, H. : Turbulence in Open-Channel Flows, IAHR-Monograph, Balkema, 1993.
7. Olsen, N. R. B. : Thee-dimensional CFD modeling of self-forming meandering channel, *J. Hydr. Eng.*, Vol.129, No.5, pp.366-372, 2003.
8. Wu, W., Rodi, W. and Wenka, T.: 3D numerical modeling of flow and sediment transport in open-channels, *J. Hydr. Eng.*, Vol.126, No.1, pp.4-15, 2000.
9. Yabe, T., Ishikawa, T., Wang, P.Y., Aoki, T., Kadota, Y. and Ikeda, F.: A universal solver for hyperbolic-equations by cubic-polynomial interpolation. II. Two- and three-dimensional solvers, *Comput. Phys. Commun.* Vol.66, pp.233-242, 1991.
10. Yabe, T., Mizoe, H. Takizawa, K., Moriki, H. Im, H. and Ogata, Y.: Higher-order schemes with CIP method and adaptive Soroban grid towards mesh-free scheme, *J. Comput. Phys.*, Vol.194, pp57-77, 2004.
11. Ye, J. and McCorquodale, J.A.: Depth-averaged hydrodynamic model in curvilinear collocated grid, *J. Hydr. Eng.*,

Vol.123, No.5, pp.380-388, 1997.

12. Zalesak, S. T.: Fully multi-dimensional flux-corrected transport algorithms for fluids. *J. Comput. Phys.*, Vol.31, 335-362, 1979.

APPENDIX – NOTATION

The following symbols are used in this paper:

D_h = horizontal kinematic eddy viscosity;

f = scalar value in pure convection problem;

F = conservation factor;

g = gravity acceleration;

h = local water depth;

H = water level;

(i, j) = two-dimensional index defined in the computation domain;

J = Jacobian defined as $J = 1/\left(x_\xi y_\eta - x_\eta y_\xi\right)$;

k = depth-averaged turbulent kinematic energy;

M, N = $x-$ and $y-$ components of discharge flux;

n_k = the value of the n axis at the side-wall ($k = right\ or\ left$);

N_x, N_y = two-dimensional grid numbers;

Q = water discharge at each section of the channel;

Q^ξ, Q^η = contravariant components of discharge fluxes;

s, n = orthogonal curvilinear coordinates;

t = time;

u , v = s - and n - components of velocity vectors;

U , V = x - and y - components of velocity vectors;

$\widehat{U}$, $\widehat{V}$ = contravariant components of velocity vectors;

U_* = local friction velocity;

$\widetilde{\overline{-u_i'u_j'}}$ = orthogonal curvilinear components of depth-averaged Reynolds stress tensors;

$\widetilde{\overline{-U_i'U_j'}}$ = Cartesian components of depth-averaged Reynolds stress tensors;

x , y = Cartesian coordinates;

ε = prescribed threshold value in the iterative computation;

λ = deviation factor which estimates the difference between each numerical value and the theoretical value;

ξ, η = boundary fitted coordinates;

$\xi_x, \eta_x, \xi_y, \eta_y$ = metrics, for instance, $\xi_x = \partial\xi / \partial x$;

ρ = fluid density;

σ = local curvature along the channel coordinate (s axis);

τ_{bx} , τ_{by} = x - and y - components of bottom shear stress vectors;

τ_{bs} , τ_{bn} = s - and n - components of bottom shear stress vectors;

τ_b^{ξ} , τ_b^{η} = contravariant components of bottom shear stress vectors;

superscript $'$ = the time fluctuation component;

superscript $\bar{}$ = the time-averaging operator;

superscript $\bar{=}$ = the cross-sectionally averaging operator;

superscript $\tilde{}$ = the depth-averaging operator;

superscript * = the time level when the physical values are computed in an advection phase of the CIP scheme;

superscript ** = the time level when the provisional values are computed without the water level gradient term;

superscript n = the time level at $n\Delta t$ (Δt = time increment);

superscript n+1 = the time level at $(n+1)\Delta t$;

suffix *cal* = the calculated values

suffix *in* = the values observed in the upstream end or inlet of the channel

suffix *ini* = the initial values

suffix *theory* = the theoretical values; and

suffix *out* = the values observed in the downstream end or outlet of the channel.

(Received Jun 13, 2007 ; revised Sep 06, 2007)